ARTICLE

Imogolite Nanotubes: Stability, Electronic, and Mechanical Properties

Luciana Guimarães,[†,‡] Andrey N. Enyashin,[‡,§] Johannes Frenzel,[‡] Thomas Heine,[‡,*] Hélio A. Duarte,[†] and Gotthard Seifert[‡]

[†]Grupo de Pesquisa em Química Inorgânica Teórica, Departamento de Química-ICEx- Universidade Federal de Minas Gerais, 31.270-901 Belo Horizonte, MG, Brazil, [‡]Department of Physical Chemistry, Technische Universität Dresden, D-01062 Dresden, Germany, and [§]Institute of Solid State Chemistry, Ural Branch of the Russian Academy of Science, 620219 Ekaterinburg, Russian Federation

ABSTRACT The aluminosilicate mineral imogolite is composed of single-walled nanotubes with stoichiometry of $(HO)_3Al_2O_3SiOH$ and occurs naturally in soils of volcanic origin. In the present work we study the stability and the electronic and mechanical properties of *zigzag* and armchair imogolite nanotubes using the density-functional tight-binding method. The (12,0) imogolite tube has the highest stability of all tubes studied here. Uniquely for nanotubes, imogolite has a minimum in the strain energy for the optimum structure. This is in agreement with experimental data, as shown by comparison with the simulated X-ray diffraction spectrum. An analysis of the electronic densities of states shows that all imogolite tubes, independent on their chirality and size, are insulators.

KEYWORDS: inorganic nanotubes · strain energy · DFTB · aluminosilicate · XRD

Nanotubes (NTs) have been increasingly investigated in the past decade and have become a symbol of the new and fast developing area of nanotechnology.[1] The widespread attention can be traced not only to their interesting structure but also to their wide range of electrical, chemical, and mechanical properties. Since the discovery of inorganic nanotubes[2] (WS_2) in 1992, many other inorganic nanotubes have been reported, based on transition metal chalcogenides,[2,3] boron nitride- and silicon oxide-based NTs,[4,5] transition metal oxides,[6,7] and others.

The aluminosilicate mineral imogolite occurs naturally in soils of volcanic origin and is composed of single-walled nanotubes. The tube walls consist of a curved gibbsite-like sheet ($Al(OH)_3$), where the inner hydroxyl surface of the gibbsite is substituted by (SiO_3)OH groups. This structure possesses a composition of $(HO)_3Al_2O_3SiOH$,[8] which is the sequence of atoms encountered on passing from the outer to the inner surface of the tube (Figure 1a).

Imogolite NTs have specific characteristics as well as defined tube length and diameter that make them unique in comparison to other NTs. In general, it remains a challenge in the synthesis of nanoparticles to control the dimensions and produce monodisperse NTs. Moreover, various theoretical studies on several nanotubes, such as C,[9,10] BN,[9,10] BC_2N,[9] GaS,[11] MoS_2,[12] and TiO_2,[13] have shown that the strain energy necessary to roll a monolayer into a tube decreases monotonically with increasing tube radius. Therefore, there is no suitable energy minimum that could be employed to produce nanotubes with a desired diameter.[14] However, the imogolite type is an apparent exception.[15–17] As shown in Fig-

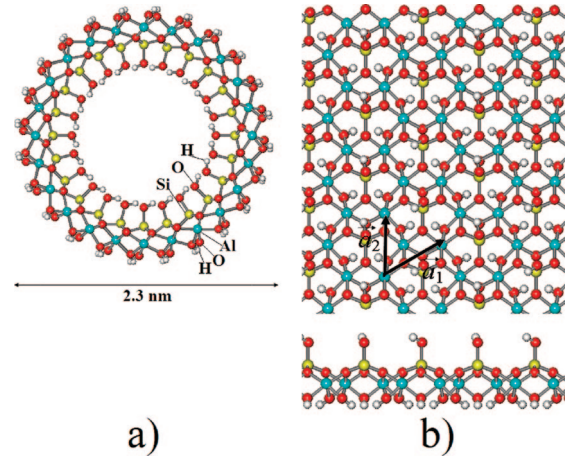

Figure 1. (a) Cross section view of imogolite showing composition. (b) Optimized structure of hypothetical 2D imogolite layer with lattice vectors $\mathbf{a}_1$ and $\mathbf{a}_2$; views from the top and from the side are shown. White atoms, H; red, O; gray, Al; yellow, Si.

*Address correspondence to thomas.heine@chemie.tu-dresden.de.

Received for review August 21, 2007 and accepted October 11, 2007.

Published online November 30, 2007. 10.1021/nn700184k CCC: $37.00

ure 1a, the external tube diameter is around 2.3 nm, while the internal diameter is around 1.0 nm. The average length of imogolite nanotubes is ~100 nm,[16] and the length of the unit cell along the tube axis is 0.85 nm.

There are several experimental studies on imogolite available in the literature, and various applications, *e.g.*, as catalyst support,[18,19] molecular sieving material for membranes, adsorbents, and materials for gas storage (methane, CO_2, and N_2),[18,20,21] have been suggested. Imogolite has a refractive index similar to those of common polymers, a necessary precondition for applications as transparent polymer additives.[22] The hydroxyl groups offer interesting applications as proton conductors and ion retention and channel devices.[23]

However, only a few theoretical studies of imogolite nanotubes have been carried out. Due to the size of the unit cell, with several hundreds of atoms, these studies have been restricted to classical molecular dynamics simulations using empirical potentials and are therefore restricted to investigations of the mechanical properties of imogolite nanotubes.[14,24]

Two molecular mechanics simulations, one using a many-body potential[24] with specific parameters for imogolite and one employing the CLAYFF force field,[14] reported the existence of a minimum of the strain energy per atom depending on the tube radius for imogolite, which makes them unique among NTs. According to experiments,[16] the circumference of imogolite is composed of 12 gibbsite units. The results obtained with the CLAYFF force field[14] reproduce this experimental result, whereas Tamura *et al.*[24] reported, on the basis of simulations using their many-body potential, 16 gibbsite units in the tube circumference for the optimal imogolite tube.

In this work we study the geometry and the electronic structure of imogolite on the basis of a quantum-mechanical approach. We scan the properties for various chiralities and sizes of the tubes. Our results will extend the theoretical understanding of this material, in particular in the perspective of potential technological applications.

RESULTS AND DISCUSSION

The topologies of all investigated imogolite tubes have been maintained during full optimization of the geometries starting from the initial structures. This indicates that the cylindrical modification is a stable local minimum for this stoichiometry. Figure 2 illustrates the minimum energy structures found for the (12,0) *zigzag* and (8,8) *armchair* imogolite nanotubes. In addition, we performed molecular dynamics simulations at 300 K, which confirm the stability of the tubular structure.

The average Al−O, Si−O, and Al−Al bond lengths are 1.89, 1.68, and 2.92 Å, respectively, for the (12,0) nanotube and differ only by ±0.01 Å for the other studied chiralities. The calculated bond distances are in close agreement with reported X-ray data (1.86 and 1.63 Å for Al−O and Si−O distances, respectively).[8]

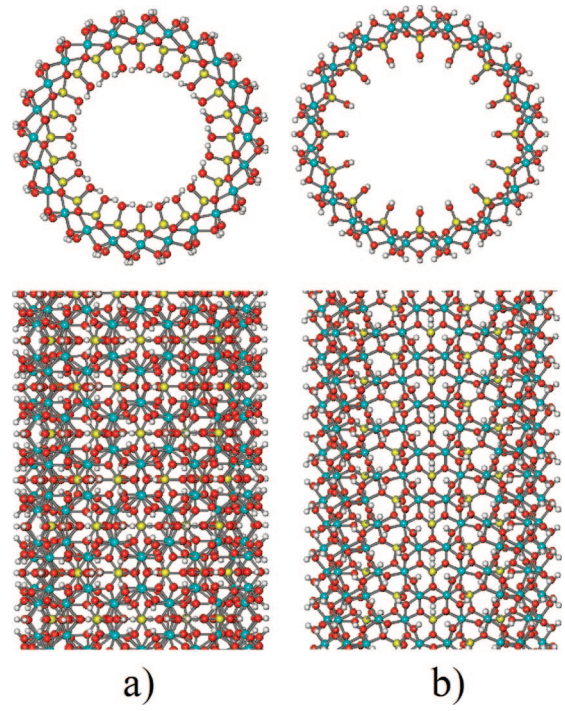

Figure 2. Optimized structures of *zigzag* (12,0) (a) and *armchair* (8,8) (b) imogolite nanotubes. White atoms, H; red, O; blue, Al; yellow, Si.

X-ray and electron diffraction structure analyses for imogolite were first reported in 1972 by Cradwick *et al.*,[8] who pointed out that the circumference of natural imogolite is composed by 10 gibbsite units. In contrast, the first imogolite tubes synthesized by Farmer and Fraser in 1977[17] contained 12 gibbsite units around the circumference, as shown by X-ray analysis.[17,25] Most strikingly, the synthetic tubes are of (12,0) topology, and no tubes of different chiralities have been observed.

We have simulated the X-ray diffraction (XRD) spectra for different tubes using the optimized density-functional tight-binding (DFTB) geometries and compared them with experimental data. The XRD simulations were carried out assuming that the material is composed of randomly oriented nanotubes of same structure and size. The average scattering power I, in electron units, is given by the Debye formula (eq 1), where r_{ij} is the distance between the ith and jth atoms, and f_i and f_j are the atomic scattering factors of the ith and jth atoms. s is the X-ray scattering vector, and $s = 4\pi \sin\theta/\lambda$, with the diffraction angle 2θ and the X-ray wavelength λ (in this work, $\lambda = 1.542$ Å, like for nickel-filtered Cu Kα radiation). The values of the atomic scattering factors were taken from *International Tables for Crystallography*.[26]

$$I(s) = \sum_i \sum_j f_i f_j \frac{\sin(sr_{ij})}{sr_{ij}} \qquad (1)$$

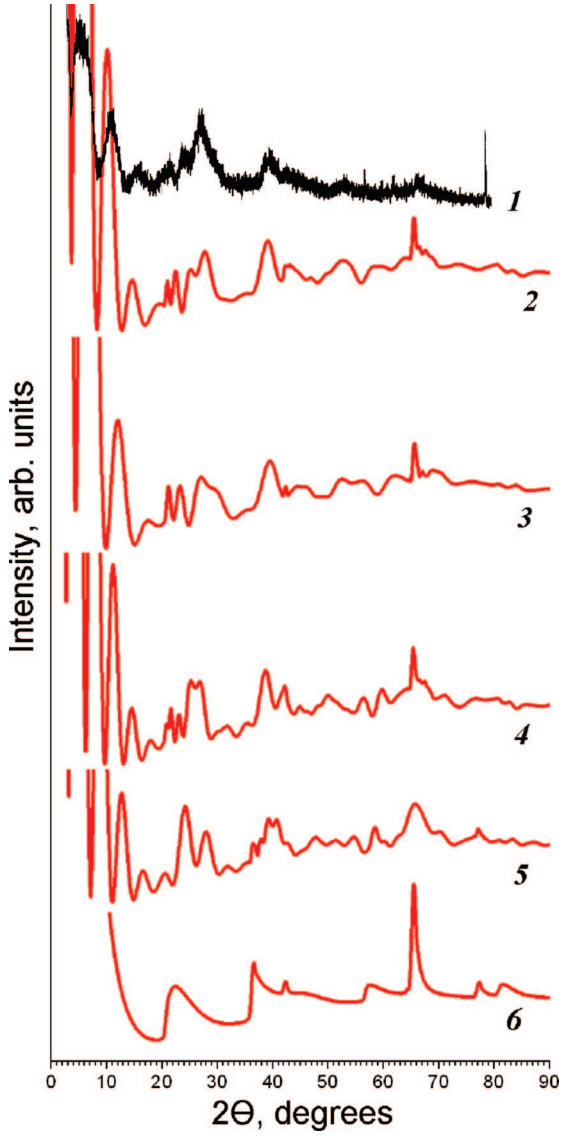

Figure 3. Experimental and simulated XRD spectra imogolite nanotubes: (1) experimental,[18] (2) (12,0) zigzag nanotube, (3) (10,0) zigzag nanotube, (4) (16,0) zigzag nanotube, (5) (8,8) armchair nanotube, and (6) hypothetical 2D imogolite layer.

The XRD spectrum of the synthesized imogolite nanotube[18] has been compared with the simulated spectra for the (10,0), (12,0), (16,0), (8,8), and 2D imogolite layers, as depicted in Figure 3. The (12,0) and (8,8) structures have been chosen for their high stability, the (10,0) tube due to the early study of Cradwick *et al.*,[8] presenting this structure as naturally occurring imogolite, and the (16,0) configuration to analyze the most stable tube pointed out by Tamura *et al.*[24] The results obtained for the (16,0) and (8,8) tubes give a slightly different profile, compared to the experimental spectrum, while the profile of the 2D imogolite layer is clearly different. For the (16,0) and (8,8) tubes, more peaks in the very low angle range are observed, suggesting a dependence of these peaks on the chirality of the tubes.

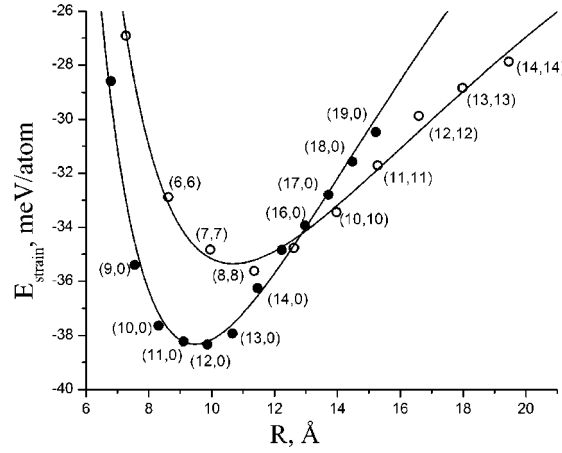

Figure 4. Calculated strain energies E_{str} as a function of the radius R for zigzag (●) and armchair (○) imogolite nanotubes.

For the (12,0) configuration, the positions of the calculated peaks at $2\theta = 5°$, 10°, and 15° match well with the experimental spectrum. A similar pattern is observed for the (10,0) tube, with small differences for $2\theta = 15°$ and $2\theta \approx 30°$.

The XRD simulations support the presence of (12,0) imogolite NT in experiments, but we cannot exclude the (10,0) configuration on this basis. However, the existence of one stable chirality of imogolite NT can be confirmed by the calculated energies of the nanotubes, as shown in the next section.

Energetic Properties. The calculated strain energies as a function of the tube diameter are depicted in Figure 4. The strain energies per atom are defined as the difference of the total energies between the tube and the planar layer. Generally, they reflect the energy penalty required for the rolling of the planar sheet onto a cylinder. For all NTs, this function decreases monotonically with the tube diameter as it approaches the value of the planar sheet. From Figure 4, it is evident that imogolite is an exception: it has a minimum for the (12,0) nanotube. The same result has been reported by Konduri *et al.*[14] on the basis of classical molecular dynamic simulations. The experimentally measured outer diameter of the imogolite nanotube was estimated to be about 2.3 nm, based directly on transmission electron microscopy imaging and indirectly on center-to-center distances inferred from XRD patterns.[8,15,16] We have calculated the outer diameter of (12,0) tube as 2.26 nm, taking into account the oxygen atoms on the outer surface. The same result has been reported in the literature on the basis of classical molecular dynamic simulations.[14] Moreover, Konduri *et al.*[14] developed a simplified model where the Al−O and Si−O bonds are described with harmonic bond-stretching potentials. This model explains both the strain energy minimum of imogolite and the subsequent increase of strain as a function of the tube radius.

This phenomenon, however, can also be explained in the framework of a continuum model. For several nanotubes, including C,[9,10] BN,[9,10] BC_2N,[9] GaS,[11] MoS_2,[12] and TiO_2,[13] the tube stability E_{str} (strain energy per atom) can be related to the elastic modulus Y, the thickness h of the monolayer, and the tube radius R:

$$E_{str} = \frac{a}{R^2} \sim \frac{Yh^3}{R^2} \quad (2)$$

The general trend that $E_{str} \sim a/R^2$ holds for all known nanotubes except for imogolite. For nanotubes of different compounds but with the same radius, an increase in the number of atomic planes within their walls results in larger E_{str} values; for instance, E_{str} grows in the series C $\rightarrow$ MoS_2 $\rightarrow$ GaS $\rightarrow$ AlO(OH).

Equation 2 holds for symmetric layers. In the case of imogolite—composed of a nonsymmetrical aluminosilicate layer—a difference in the surface tensions, $\Delta\sigma$, between the outer and inner tube surfaces (internal and external surface energies) must be taken into account. This result is an additional contribution to E_{str}:

$$E_{str} = \frac{a}{R^2} + \frac{b}{R} \sim \frac{Yh^3}{R^2} + \frac{\Delta\sigma \cdot h}{R} \quad (3)$$

The derivation of eq 3 is shown in the Supporting Information. The surface energy $\Delta\sigma$ supports a negative curvature, which decreases the strain energy and introduces a minimum into the $E_{str}(R)$ curve. Our DFTB calculations confirm the size dependence as given by eq 3 for zigzag and armchair imogolite nanotubes (Figure 4).

The fit of the obtained E_{str} and R values for imogolite nanotubes using eq 3 describes the change of the strain energy in the wide range of radii quite well. Zigzag nanotubes are more stable than armchair ones for $R < 12$ Å, which agrees with experiment, where no armchair nanotubes were observed. At higher radii, the stability of zigzag and armchair tubes is comparable. This energetic behavior is different for most of nanotubes, which usually have one and the same dependence of E_{str} on R, independent on their chirality.

Following Konduri *et al.*,[14] we derived an expression for the radial breathing mode (RBM) frequency by applying the harmonic approximation to eq 3:

$$\omega = \frac{2\sin(\pi/N)}{x^2}\sqrt{\frac{14N}{M}\left(6a + \frac{bx}{\sin(\pi/N)}\right)} \quad (4)$$

In eq 4, a and b are the same parameters as in eq 3, N is the number of Al atoms in the circumference, x is Al−Al distance within a tube perimeter, and M is the mass of unit cell. a and b are obtained by a least square fit of the calculated strain energies to eq 3. The RBM frequency of the nanotube as a function of the radius is depicted in Figure 5. For the (12,0) nanotube, the RBM

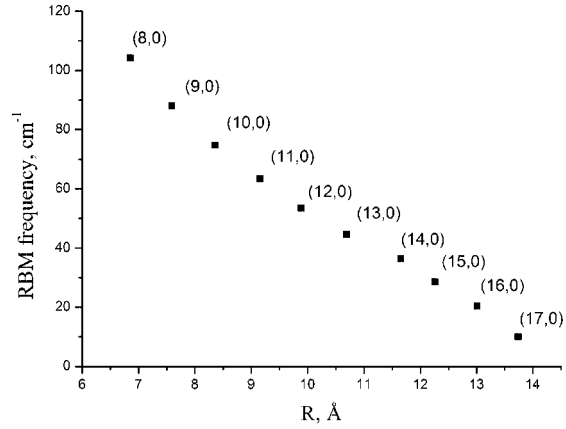

Figure 5. Radial breathing mode frequency (in cm^{-1}) for imogolite nanotubes as function of the tube radius (in Å).

frequency is 54 cm^{-1}, in good agreement with Konduri *et al.*'s[14] force field derived value of 45 cm^{-1}. The inverse dependence of the RBM frequency on the nanotube radius is also in agreement with Konduri *et al.*'s[14] observations. However, our model suggests that imogolite tubes with more than 17 gibbsite units in the circumference are instable, as eq 4 would predict imaginary frequencies of the RBM.

Electronic Properties. The electronic, optical, and mechanical properties of nanotubes may depend crucially on their chirality and diameter. For instance, the band gap value for semiconducting MoS_2 NTs[12] is determined by the tube geometry, armchair or zigzag, and tends to vanish for very small NT diameters.

Imogolite is an aluminosilicate, a class of materials well-known as insulators. Indeed, a large band gap has been reported for related α-Al_2O_3(8.75 eV in experiment and 7.77 eV calculated using GGA-DFT[27]). In the gibbsite structure, the band gap is even about 2 eV higher.[27,28] Bursill *et al.*[15] pointed out that one may expect intuitively a relatively wide band gap for imogolite. Our DFTB calculations confirm this proposition. All imogolite nanostructures considered in this study are insulators with a wide band gap. Independent of the specific chirality of the optimized *zigzag and armchair* NTs, their band gaps are around 10 eV (Table 1), and a similar value is found for the 2D imogolite layer (~10 eV). From our experience, DFTB overestimates band gaps of insulators, depending on the employed basis set and the composition of the lowest unoccupied states. On the other hand, DFT is known to underestimate insulator band gaps. On the basis of a recently reported value of 4.7 eV based on GGA-DFT calculations,[29] we estimate the correct band gap between these two values.

The total densities of states (DOS) for the most stable zigzag and armchair configurations, (12,0) and (8,8), are shown in Figure 6 (for partial DOS, see Figure S1 in the Supporting Information). The main features of the DOS plots are quite similar for all tubes and also similar to those of the hypothetical 2D imogolite layer. The valence bands of both nanotubes are composed mainly

TABLE 1. Structural, Electronic, and Elastic Properties of Imogolite Nanotubes

index	cell size/atoms	$R_{eq\ Al}$/Å	BG/eV	Y/GPa
		Imogolite (*n*,0)		
(8,0)	224	6.79	10.3	365
(9,0)	252	7.55	10.3	277
(10,0)	280	8.31	10.3	196
(11,0)	308	9.10	10.3	366
(12,0)	336	9.86	10.3	242
(13,0)	364	10.66	10.3	255
(14,0)	392	11.46	10.3	290
(15,0)	420	12.23	10.2	319
(16,0)	448	12.98	10.2	175
(17,0)	476	13.72	10.2	314
(18,0)	504	14.48	10.2	202
(19,0)	532	15.23	10.1	479
		Imogolite (*n*,*n*)		
(5,5)	140	7.27	10.6	287
(6,6)	168	8.62	10.6	387
(7,7)	196	9.95	10.6	368
(8,8)	224	11.35	10.6	329
(9,9)	252	12.62	10.6	416
(10,10)	280	13.98	10.6	287
(11,11)	308	15.28	10.6	280
(12,12)	336	16.59	10.6	296
(13,13)	364	17.98	10.6	292
(14,14)	392	19.45	10.5	291
2D layer			10.7	

of 2p O states, and the lower part of the conduction band is formed by 3p and 3d Si states and 3d Al states.

The charge transfer from aluminium ($Q \approx +0.6e$) to oxygen ($Q \approx -0.45e$) and from silicon ($Q \approx +0.8e$) to oxygen ($Q \approx -0.54e$) is almost the same for all nanotubes, independent of the configuration and the tube radii. For more details, see Table S1 in the Supporting Information. The charge transfer from aluminium to oxygen is in the same order as in single-walled hydroxyalumina nanotubes.[30] The absolute charge values of hydrogen atoms on the inner surface are ~6% bigger

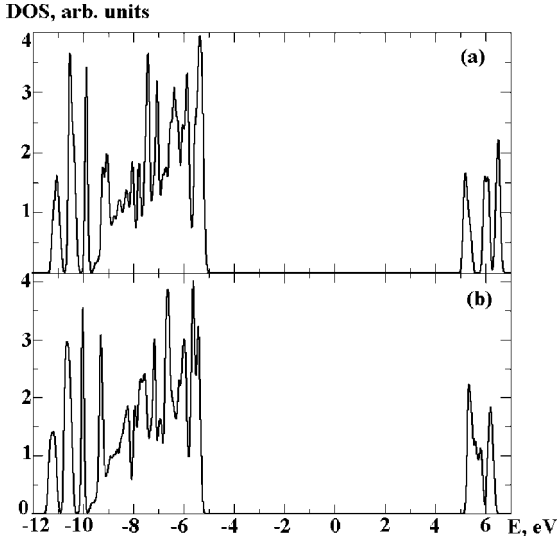

Figure 6. Total densities of states for (a) (12,0) and (b) (8,8) imogolite nanotubes after geometry optimization. All energies are given relative to the Fermi level. (See partial DOS in the Supporting Information.)

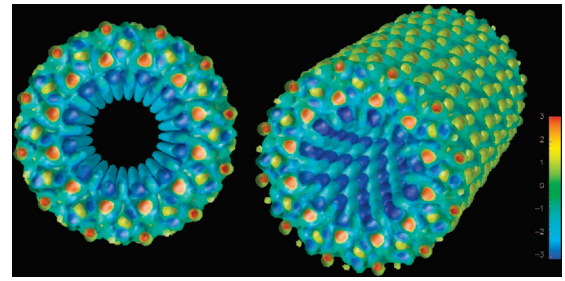

Figure 7. Electrostatic field of (12,0) imogolite nanotube: views along and diagonal to the tube axis. Different colors show equipotential surfaces: −3.0, −2.0, −1.0, +1.0, +2.0, and +3.0 e/Å.

than on the outer surface. This means that OH(Si) bonds are more ionic than OH(Al), and their acidity could be higher.

Using the optimized geometry of the (12,0) imogolite nanotube and the calculated atomic Mulliken charges, we have estimated the electrostatic field (Figure 7). This picture clearly expresses the charge distribution within the tube: mainly negative charges are present on the inner region, while positive charges are located on the outer surface.

Our DFTB results corroborate the experimental results of Gustafsson,[31] even though he did not use a (12,0) imogolite nanotube for his model approach. According to him, a weak positive charge exists on the outer wall surface of imogolite, whereas a negative charge appears in the inner surface of walls. The lack of a more precise structure of imogolite prevented Gustafsson[31] from testing his hypothesis in more detail. Our results confirm his proposition of the charge distribution. However, it is important to note that our calculations are performed in a vacuum, whereas the surface charge distribution can depend on pH, temperature, and other factors. Nevertheless, our result may be valid for the neutral form of imogolite, which is present in water solutions with a pH up to ~8.

This interesting property of imogolite nanotubes may be promising for the design of ion transport devices, as one may expect the ionic transport is guided along the tube axis.

Mechanical Properties. Knowledge of the mechanical properties of materials is essential for the development of many applications. The central property characterizing the stiffness of nanotubes, which is accessible in experiments, is the Young's modulus. The mechanical properties of nanotubes have been also estimated by theoretical works.[9,10,32,33] The Young's moduli of imogolite nanotubes have been calculated as described in the literature,[9] by performing a series of relaxation calculations for different values of the cell length in the direction of the tube axis, and thus imposing either tensile or compressive strain on the nanotube. It is then possible to calculate the second derivative of the total energy with respect to the axial strain, which enables us to calculate the Young's modulus, as given by eq 5:

$$Y = \frac{1}{V_o}\left(\frac{\partial^2 E}{\partial \epsilon^2}\right)_{\epsilon=0} \quad (5)$$

where V_o is the equilibrium volume, ϵ the strain, and the E the total energy.

The results obtained for zigzag and armchair configurations are listed in Table 1. The imogolite nanotubes have Young's moduli which fall in the range 175–390 GPa. In comparison to refs 9 and 10, we conclude that imogolite nanotubes are less stiff than other types of nanotubes, such as C,[10] BN,[10] BC_3,[10] and BC_2N,[9] but their Young's moduli are in the same order of magnitude as for MoS_2 (~230 GPa),[33] GaS (~270 GPa),[11] and chrysotile nanotubes (159 ± 125 GPa).[34]

CONCLUSIONS

Density-functional-based calculations of imogolite nanotubes explain the selectivity of a particular chirality, (12,0), for imogolite, which is different from conventional carbon and inorganic nanotubes. *Armchair* imogolite nanotubes, not detected in experiments, were also investigated. The (8,8) configuration was found to be the most stable for armchair, but clearly less stable than the (12,0) zigzag nanotube.

Comparison of experimental and simulated XRD spectra as well as the energetic results clearly indicated the presence of only (12,0) imogolite nanotubes in experiments. The appearance of (10,0) nanotubes in nature, as claimed in earlier work by Cradwick *et al.*,[8] should therefore, in our opinion, be re-examined.

All imogolite nanotubes have a wide band gap, ~10 eV, independent on their chirality. We have also shown that the imogolite nanotubes are less stiff than other types of nanotubes, including C and BN nanotubes.

Imogolite nanotubes are interesting examples of layered heterophase nanotubular systems. Our results extend the theoretical understanding of this material and also provide a perspective of potential applications. Investigations of their stability can help in the fabrication of similar systems, for instance, by scrolling into nanotubes of a few monolayers of different III−V semiconductors.

The study of growth of imogolite nanotubes is in progress.

COMPUTATIONAL DETAILS

All calculations have been carried out using the self-consistent charge density-functional-based tight-binding (SCC-DFTB) method as implemented in deMon.[35–37] This method uses a minimal set of atomic basis functions and tight-binding-like approximations to the Hamiltonian and can be applied for periodic and cluster computations. It has recently been shown that SCC-DFTB gives results in good agreement with GGA-DFT for structure and electronic properties of Gibbsite and α-aluminum oxide.[28] Frenzel *et al.*[28] showed that the electronic DOS computed with DFTB shows all features of the DOS calculated using GGA-DFT. Periodic boundary conditions were applied to the cells along tube axes.

Initial configurations of the nanotubes were constructed by folding the hypothetical 2D imogolite layer, where hydroxyl groups surrounding one vacant site of the gibbsite layer are replaced by orthosilicate anions (Figure 1b). We adopt the same convention for labeling these tubes as that used for carbon, BN, and metal chalcogenide nanotubes.[38] Depending on the rolling direction **B** in the 2D lattice, where $\mathbf{B} = n\mathbf{a}_1 + m\mathbf{a}_2$ ($\mathbf{a}_1$, $\mathbf{a}_2$ are lattice vectors of the hexagonal lattice), three classes of nanotubes can be constructed: armchair (n,n), zigzag (n,0), and "chiral" nanotubes (n,m), with $n \neq m$. We have considered zigzag and armchair NTs with diameters ranging from 13 to 40 Å, which correspond to (8,0)...(19,0) and (5,5)...(14,14) configurations. Initial structures have been fully optimized, including the internal positions and the tube lengths.

Acknowledgment. This research was supported by Coordenação de Aperfeiçoamento de Pessoal de Nível Superior (CAPES), Brazil, in cooperation with Deutscher Akademischer Austauschdienst (DAAD) and Deutsche Forschungsgemeinschaft (DFG). The authors thank Mathias Rapacioli and Agnieszka Kuc for helpful and interesting discussions.

Supporting Information Available: Derivation of eq 3, partial density of states for (12,0) and (8,8) imogolite nano - tubes, and Mulliken charges of imogolite nanotubes. This information is available free of charge *via* the Internet at http://pubs.acs.org.

REFERENCES AND NOTES

1. Saito, R.; Dresselhaus, M. S.; Dresselhaus, G. *Physical Properties of Carbon Nanotubes*; Imperial College Press: London, 1998; p 272.
2. Tenne, R.; Margulis, L.; Genut, M.; Hodes, G. Polyhedral and Cylindrical Structures of Tungsten Disulfide. *Nature* **1992**, *360*, 444–446.
3. Feldman, Y.; Wasserman, E.; Srolovitz, D. J.; Tenne, R. High-Rate, Gas-Phase Growth of Mos_2 Nested Inorganic Fullerenes and Nanotubes. *Science* **1995**, *267*, 222–225.
4. Sha, J.; Niu, J. J.; Ma, X. Y.; Xu, J.; Zhang, X. B.; Yang, Q.; Yang, D. Silicon Nanotubes. *Adv. Mater.* **2002**, *14*, 1219.
5. Chopra, N. G.; Luyken, R. J.; Cherrey, K.; Crespi, V. H.; Cohen, M. L.; Louie, S. G.; Zettl, A. Boron-Nitride Nanotubes. *Science* **1995**, *269*, 966–967.
6. Pu, L.; Bao, X. M.; Zou, J. P.; Feng, D. Individual Alumina Nanotubes. *Angew. Chem., Int. Ed.* **2001**, *40*, 1490.
7. Hoyer, P. Formation of a Titanium Dioxide Nanotube Array. *Langmuir* **1996**, *12*, 1411–1413.
8. Cradwick, P. D.; Wada, K.; Russell, J. D.; Yoshinag; N.; Masson, C. R.; Farmer, V. C. Imogolite, a Hydrated Aluminum Silicate of Tubular Structure. *Nature (London), Phys. Sci.* **1972**, *240*, 187–189.
9. Hernandez, E.; Goze, C.; Bernier, P.; Rubio, A. Elastic Properties of C and $B_xC_yN_z$ Composite Nanotubes. *Phys. Rev. Lett.* **1998**, *80*, 4502–4505.
10. Hernandez, E.; Goze, C.; Bernier, P.; Rubio, A. Elastic Properties of Single-Wall Nanotubes. *Appl. Phys. A* **1999**, *68*, 287–292.
11. Köhler, T.; Frauenheim, T.; Hajnal, Z.; Seifert, G. Tubular Structures of GaS. *Phys. Rev. B* **2004**, 69.
12. Seifert, G.; Terrones, H.; Terrones, M.; Jungnickel, G.; Frauenheim, T. Structure and Electronic Properties of MoS2 Nanotubes. *Phys. Rev. Lett.* **2000**, *85*, 146–149.
13. Enyashin, A. N.; Seifert, G. Structure, Stability and Electronic Properties of TiO^2 Nanostructures. *Phys. Status Solidi B* **2005**, *242*, 1361–1370.
14. Konduri, S.; Mukherjee, S.; Nair, S. Strain Energy Minimum and Vibrational Properties of Single-Walled Aluminosilicate Nanotubes. *Phys. Rev. B* **2006**, *74*, 033401.

15. Bursill, L. A.; Peng, J. L.; Bourgeois, L. N. Imogolite: An Aluminosilicate Nanotube Material. *Philos. Mag. A* **2000**, *80*, 105–117.
16. Mukherjee, S.; Bartlow, V. A.; Nair, S. Phenomenology of the Growth of Single-Walled Aluminosilicate and Aluminogermanate Nanotubes of Precise Dimensions. *Chem. Mater.* **2005**, *17*, 4900–4909.
17. Farmer, V. C.; Fraser, A. R.; Tait, J. M. Synthesis of Imogolite−Tubular Aluminum Silicate Polymer. *J. Chem. Soc., Chem. Commun.* **1977**, 462–463.
18. Ohashi, F.; Tomura, S.; Akaku, K.; Hayashi, S.; Wada, S. I. Characterization of Synthetic Imogolite Nanotubes as Gas Storage. *J. Mater. Sci.* **2004**, *39*, 1799–1801.
19. Farmer, V. C.; Adams, M. J.; Fraser, A. R.; Palmieri, F. Synthetic Imogolite−Properties, Synthesis, and Possible Applications. *Clay Miner.* **1983**, *18*, 459–472.
20. Ackerman, W. C.; Smith, D. M.; Huling, J. C.; Kim, Y. W.; Bailey, J. K.; Brinker, C. J. Gas Vapor Adsorption in Imogolite−A Microporous Tubular Aluminosilicate. *Langmuir* **1993**, *9*, 1051–1057.
21. Pohl, P. I.; Faulon, J. L.; Smith, D. M. Pore Structure of Imogolite Computer Models. *Langmuir* **1996**, *12*, 4463–4468.
22. Yamamoto, K.; Otsuka, H.; Takahara, A. Preparation of Novel Polymer Hybrids From Imogolite Nanofiber. *Polym. J.* **2007**, *39*, 1–15.
23. Su, C. M.; Harsh, J. B. The Electrophoretic Mobility of Imogolite and Allophane in the Presence of Inorganic Anions and Citrate. *Clays Clay Miner.* **1993**, *41*, 461–471.
24. Tamura, K.; Kawamura, K. Molecular Dynamics Modeling of Tubular Aluminum Silicate: Imogolite. *J. Phys. Chem. B* **2002**, *106*, 271–278.
25. Farmer, V. C.; Fraser, A. R.; Tait, J. M.; Palmieri, F.; Violante, P.; Nakai, M.; Yoshinaga, N. Imogolite and Proto-Imogolite in an Italian Soil Developed on Volcanic Ash. *Clay Miner.* **1978**, *13*, 271–274.
26. *International Tables For Crystallography*; Prince, E., Ed.; Kluwer Academic Publishers: Dordrecht/Boston/London, 2004; Vol. C, pp 554–564.
27. Lodziana, Z.; Norskov, J. K. Adsorption of Cu and Pd on Alpha-Al_2O_3(0001) Surfaces with Different Stoichiometries. *J. Chem. Phys.* **2001**, *115*, 11261–11267.
28. Frenzel, J.; Oliveira, A. F.; Duarte, H. A.; Heine, T.; Seifert, G. Structural and Electronic Properties of Bulk Gibbsite and Gibbsite Surfaces. *Z. Anorg. Allg. Chem.* **2005**, *631*, 1267–1271.
29. Alvarez-Ramirez, F. Ab Initio Simulation of the Structural and Electronic Properties of Aluminosilicate and Aluminogermanate Nanotubes with Imogolite-Like Structure. *Phys. Rev. B* **2007**, *76*, 125421.
30. Enyashin, A. N.; Ivanovskii, A. L.; Seifert, G. Stability and Electronic Properties of Single-Walled Gamma-AlO(OH) Nanotubes. *Mendeleev Commun.* **2006**, 292–294.
31. Gustafsson, J. P. The Surface Chemistry of Imogolite. *Clays Clay Miner.* **2001**, *49*, 73–80.
32. Kaplan-Ashiri, I.; Cohen, S. R.; Gartsman, K.; Ivanovskaya, V.; Heine, T.; Seifert, G.; Wiesel, I.; Wagner, H. D.; Tenne, R. On the Mechanical Behavior of WS_2 Nanotubes Under Axial Tension and Compression. *Proc. Natl. Acad. Sci. U.S.A.* **2006**, *103*, 523–528.
33. Kaplan-Ashiri, I.; Cohen, S. R.; Gartsman, K.; Rosentsveig, R.; Seifert, G.; Tenne, R. Mechanical Behavior of Individual WS_2 Nanotubes. *J. Mater. Res.* **2004**, *19*, 454–459.
34. Piperno, S.; Santucci, S.; Kaplan-Ashiri, I.; Cohen, S. R.; Popovitz-Biro, R.; Wagner, D. H.; Tenne, R.; Foresti, E.; Lesci, I. G.; Roveri, N. Mechanical Characterization of Geoinspired and Synthetic Chrysotile Nanotubes by Atomic Force Microscopy. Manuscript in preparation.
35. Elstner, M.; Porezag, D.; Jungnickel, G.; Elsner, J.; Haugk, M.; Frauenheim, T.; Suhai, S.; Seifert, G. Self-Consistent-Charge Density-Functional Tight-Binding Method for Simulations of Complex Materials Properties. *Phys. Rev. B* **1998**, *58*, 7260–7268.
36. Seifert, G.; Porezag, D.; Frauenheim, T. Calculations of Molecules, Clusters, and Solids with a Simplified LCAO-DFT-LDA Scheme. *Int. J. Quantum Chem.* **1996**, *58*, 185–192.
37. Köster, A. M.; Flores, R.; Geudtner, G.; Goursot, A.; Heine, T.; Patchkovskii, S.; Reveles, J. U.; Vela, A., Salahub, D. *deMon*, Version 1.2; NRC: Ottawa, 2004.
38. Dresselhaus, M. S.; Dresselhaus, G.; Saito, R. Carbon-Fibers Based on C-60 and Their Symmetry. *Phys. Rev. B* **1992**, *45*, 6234–6242.